Adaptive exponential integrate-and-fire model with fractal extension ⊘

Diogo L. M. Souza ⓘD ; Enrique C. Gabrick ⓘD ; Paulo R. Protachevicz ✉ ⓘD ; Fernando S. Borges ⓘD ;
José Trobia ⓘD ; Kelly C. Iarosz ⓘD ; Antonio M. Batista ⓘD ; Iberê L. Caldas ⓘD ; Ervin K. Lenzi ⓘD

Check for updates

View Online

Export Citation

12 August 2024 20:53:05

Chaos

Special Topic:
Anomalous Diffusion and Fluctuations
in Complex Systems and Networks

Submit Today

AIP Publishing

Adaptive exponential integrate-and-fire model with fractal extension

View Online   Export Citation   CrossMark

Diogo L. M. Souza,[1] Enrique C. Gabrick,[1,2,3] Paulo R. Protachevicz,[4,a] Fernando S. Borges,[5,6]
José Trobia,[7] Kelly C. Iarosz,[8] Antonio M. Batista,[1,4,7] Iberê L. Caldas,[4] and Ervin K. Lenzi[1,9]

AFFILIATIONS

[1] Graduate Program in Science, State University of Ponta Grossa, 84030-900 Ponta Grossa, PR, Brazil
[2] Department of Physics, Humboldt University Berlin, Newtonstraße 15, 12489 Berlin, Germany
[3] Potsdam Institute for Climate Impact Research, Telegrafenberg A31, 14473 Potsdam, Germany
[4] Institute of Physics, University of São Paulo, 05508-090 São Paulo, SP, Brazil
[5] Department of Physiology and Pharmacology, State University of New York Downstate Health Sciences University, Brooklyn, New York 11203, USA
[6] Center for Mathematics, Computation, and Cognition, Federal University of ABC, 09606-045 São Bernardo do Campo, SP, Brazil
[7] Department of Mathematics and Statistics, State University of Ponta Grossa, 84030-900 Ponta Grossa, Brazil
[8] University Center UNIFATEB, 84266-010 Telêmaco Borba, PR, Brazil
[9] Departament of Physics, State University of Ponta Grossa, Av. Gen. Carlos Cavalcanti 4748, Ponta Grossa 84030-900, PR, Brazil

Note: This paper is part of the Focus Issue: Data-Driven Models and Analysis of Complex Systems.
[a] Author to whom correspondence should be addressed: protachevicz@gmail.com

ABSTRACT

The description of neuronal activity has been of great importance in neuroscience. In this field, mathematical models are useful to describe the electrophysical behavior of neurons. One successful model used for this purpose is the Adaptive Exponential Integrate-and-Fire (Adex), which is composed of two ordinary differential equations. Usually, this model is considered in the standard formulation, i.e., with integer order derivatives. In this work, we propose and study the fractal extension of Adex model, which in simple terms corresponds to replacing the integer derivative by non-integer. As non-integer operators, we choose the fractal derivatives. We explore the effects of equal and different orders of fractal derivatives in the firing patterns and mean frequency of the neuron described by the Adex model. Previous results suggest that fractal derivatives can provide a more realistic representation due to the fact that the standard operators are generalized. Our findings show that the fractal order influences the inter-spike intervals and changes the mean firing frequency. In addition, the firing patterns depend not only on the neuronal parameters but also on the order of respective fractal operators. As our main conclusion, the fractal order below the unit value increases the influence of the adaptation mechanism in the spike firing patterns.

Published under an exclusive license by AIP Publishing. https://doi.org/10.1063/5.0176455

Non-integer derivatives are able to provide a more realistic representation of different dynamical systems activities due to the generalization of the derivative operator. Motivated by this, we study the dynamic behavior of the adaptive exponential integrate-and-fire model with derivative fractal extension. We observe that the neuron dynamics depend on the fractal order. Decreasing the fractal order, the adaptation and the coefficient of variation increase, as well as the firing frequency reduces. For some specific values of reset parameters, the fractal order plays a crucial role in the firing pattern. In our simulations, we show that the firing pattern is not only dependent on the reset conditions, as the standard model, but it also has a dependency on the derivative fractal order of the membrane potential and adaptation current.

I. INTRODUCTION

The description of the membrane potential is a fundamental question in neuroscience.[1] Mathematical models have been used to investigate this subject,[2] such as Hodgkin-Huxley,[3] Hindmarsh-Rose,[4] Izhikevich,[5] Lapicque integrate-and-fire (IF),[6] adaptive exponential integrate-and-fire (Adex),[7] Rulkov map,[8] among others.[9–13]

The differences among these models are in the mathematical framework, the biological description,[2] and the computational cost.[14] Usually, models with greater biological fidelity require many parameters and high computational costs. It is possible to describe the membrane potential in a really simplified way, however, sometimes with no satisfactory biological meaning. In this work, we consider the Adex model which has a good balance between the biological meaning, computational process cost, and a relatively small set of parameters.[15–17]

The Adex model was proposed in 2005 by Brette and Gerstner as an improvement of the leak conductance neuronal model.[7] Such improvement consists of the inclusion of a spike mechanism term in the potential variable and an additional variable to describe the adaptation mechanism. Besides the simplicity of this model and its low computational cost, it presents a great biophysical accuracy[2] and fits neuronal dynamics.[18] In the Adex, the membrane potential depends on the adaptation current that describes the slow activation and deactivation of some potassium ionic channels in the neuron.[19] A spike threshold mechanism, represented by an exponential term, describes the fast arising when an action potential is generated.[2,7,16] However, the exponential term introduces a discontinuity in the model which is solved considering the reset condition when the membrane potential overpasses a certain threshold. Depending on the reset condition in the potential and adaptation current, it is possible to reproduce different firing patterns.[16] Moreover, for some sets of these parameters, chaotic solutions are found.[20]

The standard description of the Adex model is based on ordinary differential equations (ODE), where the differential operators have integer order. This description has good accuracy in describing real patterns[16] and exhibits rich dynamic solutions of the neuronal activities.[21] Nonetheless, recent developments have been showing that extensions of integer operators to non-integer can increase the accuracy of the models to fit real data[22] and modify the dynamical properties.[23] The most famous non-integer extensions are the fractional operators. Fractional calculus has been used in many fields, such as quantum mechanics,[24,25] Hamiltonian systems,[26] photothermal,[27] epidemiology,[28] and others.[29–35] In the neuroscience models, fractional extensions of Hindmarsh–Rose,[36,37] Hodgkin–Huxley,[38,39] Rulkov,[40,41] and leaky integrate-and-fire[42,43] have been studied. However, the literature about fractional extensions of the Adex model is scarce. We address this lack of literature to the discontinuity of integrate-and-fire models and the difficulty to take this particularity into account in fractional derivatives. Due to fractional calculus properties, it is very hard to work with non-smooth systems. As an alternative of non-integer operators that we can employ are the fractal ones. The fractal derivative was proposed as local operators,[44] which are directly connected with the fractal dimension.[45] In this way, one form to understand the non-integer effects in the Adex model is by means of fractal derivatives.

Fractal calculus has been considered to describe many phenomena when the standard calculus fails,[46] which is based on the fractal space-time concept.[35,47,48] In the context of porous media, where the space is discontinuous, the fractal framework has presented a great description of phenomena.[49–51] In theoretical physics, fractal calculus is well explored in dark energy topics.[35] El Naschie considered the fractal space-time and pointed out that dark energy is around 95.5% of the total energy-mass of the Universe.[52,53] In the

context of diffusion process, fractal calculus is used to study the anomalous relaxation process.[33,44] In biological models, the fractal derivatives describe very well the heat conduction in the polar bear hairs.[34] In addition, when fractal derivatives are considered in the SIS epidemiological model, the description of real data increases. For example, considering Brazilian data from syphilis, it is possible to obtain a correlation coefficient equal to 0.998 with fractal operators;[54] meanwhile, the integer derivative operator produces a correlation coefficient equal to 0.990. Other applications are found in Ref. 55, where the authors showed that for some non-integer order differential operators new system properties emerge.

In this work, we study the behavior of the Adex model when it is described by fractal order differential equations. We investigate the effect of fractal order (α) with equal values in both neuronal variables (V and w) as well as in independent order in each variable. For small values of α, we show that the inter-spike intervals (ISIs) increase. The change in $\overline{\text{ISI}}$ is proportional to an exponential function of α. Furthermore, we show that the firing pattern changes when the potential membrane and the adaptation current are of two different fractal orders.

II. INTEGER ADEX MODEL

The adaptive exponential integrate-and-fire model[7] is described by the following equations:

$$C\frac{dV}{dt} = -g_L(V - E_R) + g_L\Delta_T \exp\left(\frac{V - V_T}{\Delta_T}\right) - w + I, \quad (1)$$

$$\tau_w \frac{dw}{dt} = a(V - E_R) - w, \quad (2)$$

where C is the membrane capacitance, V is the membrane potential, t is the time, g_L is the leak conductance, E_R is the rest potential, Δ_T is the slope factor, V_T is the threshold potential, w is the adaptation current, I is the injected current, τ_w is the time constant, and a is the level of sub-threshold adaptation. When V reaches a maximum value (V_{max}), the following reset conditions are applied:

$$V \to V_r, \quad (3)$$

$$w \to w_r = w + b. \quad (4)$$

For this model, we employ numerical solutions by the Runge–Kutta fourth-order method. In our simulations, we use $C = 200\,\text{pF}$, $g_L = 12\,\text{nS}$, $E_R = -70\,\text{mV}$, $\Delta_T = 2\,\text{mV}$, $V_T = -50\,\text{mV}$, $I = 512\,\text{nA}$, $a = 2\,\text{nS}$, $\tau_w = 300\,\text{ms}$, and $V_{max} = -40\,\text{mV}$.[16] The initial conditions are given by $V(0) = E_R$ and $w(0) = 0$, which correspond to a neuron initially absent of external current in a rest state.

Considering different combinations of V_r and b, it is possible to distinguish firing patterns,[17] as displayed in Table I. We identify five firing patterns, adaptation [Fig. 1(a)], tonic spiking [Fig. 1(b)], initial bursting [Fig. 1(c)], irregular bursting [Fig. 1(d)], and regular bursting [Fig. 1(e)]. In the adaptation dynamics, the inter-spike intervals (ISIs) increase throughout the time during the application of a constant current (I) due to the adaptive current mechanism. This behavior is not observed in tonic spiking, where ISI is constant. On the other hand, for initial bursting, the first ISI starts short and then increases over time. For regular bursting, the interval

TABLE I. Distinguish firing patterns depending on the reset parameters.

Firing pattern (region)	V_r (mV)	b (pA)	Fig.
Adaptation (I)	−68.0	60	1(a)
Tonic spiking (II)	−65.0	5	1(b)
Initial bursting (III)	−48.8	35	1(c)
Irregular bursting (IV)	−47.4	41	1(d)
Regular bursting (V)	−45.0	40	1(e)

between each bursting train after the transient is constant. Whereas, in irregular bursting, the interval between bursting trains is not constant.

The ISI is used to distinguish the patterns of spiking and bursting and it is defined by $\text{ISI} = t_{m+1} - t_m$, where t_m is the mth firing of each neuron. In this way, we consider the coefficient of variation (CV) of ISI, and CV is given by

$$\text{CV} = \frac{\sigma_{\text{ISI}}}{\overline{\text{ISI}}}, \tag{5}$$

where σ_{ISI} is the standard deviation of the ISI normalized by the mean inter-spike interval $\overline{\text{ISI}}$.[56] The bursting pattern produces CV ≥ 0.5 and the spiking pattern produces CV < 0.5. In the CV measure, we discard the first four ISIs that are related to transient time. To measure the mean firing frequency, we consider the definition $\overline{F} = \overline{\text{ISI}}^{-1}$.

The adaptive index is employed to distinguish adaptive and tonic spiking. The adaptive index is defined as

$$\text{A} = \frac{1}{q - d - 1} \sum_{m=q}^{d} \frac{\text{ISI}_m - \text{ISI}_{m-1}}{\text{ISI}_m + \text{ISI}_{m-1}}, \tag{6}$$

where ISI_m is the inter-spike interval between the mth and $(m+1)$th firings. Due to the numerical transient, we discard the first four ISI[16] by considering $q=4$, and d is the last ISI. To identify the adaptive or tonic firing pattern, it is necessary to define a critical value of A, which we define as $\text{A}_c = 0.01$.[16] $\text{A} > \text{A}_c$ and $-\text{A}_c \leq \text{A} \leq \text{A}_c$ characterize the adaptive and tonic spiking, respectively.
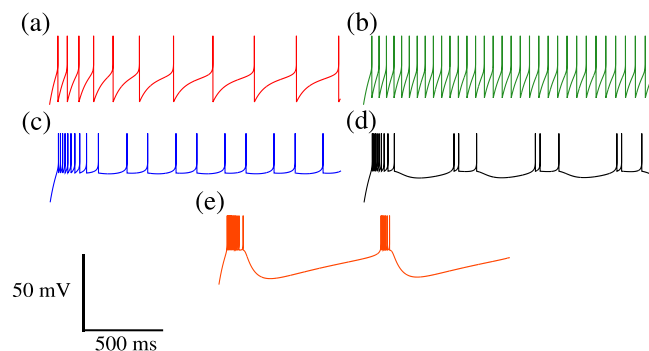
FIG. 1. Firing patterns generated by the Adex model, using reset parameters in Table I. Panels (a), (b), (c), (d), and (e) display adaptation spiking, tonic spiking, initial bursting, irregular bursting, and regular bursting, respectively.

The characterization of initial, regular, and irregular burstings is done by the analysis of the phase-space ($w \times V$) using the nullcline ($dV/dt = 0$).[16] Reset condition in the region $dV/dt > 0$ is associated with the spiking firing pattern while in the region $dV/dt < 0$ allows the emergence of the bursting firing pattern.[57] We count the number of times that $dV/dt > 0$ when the reset conditions are applied. If the amount of reset in the region $dV/dt < 0$ is the same after resets in the region $dV/dt > 0$, the firing pattern is regular bursting; otherwise, we have irregular bursting. If right after the application of the constant current, it is only counted $dV/dt > 0$ and after transient time interval we only count $dV/dt < 0$, there is an initial bursting.

Figure 2(a) displays the reset parameter space $b \times V_r$, where each pattern region is identified by different colors. The red color (region I) shows the parameter combinations that generate adaptation spiking, the green color (region II) exhibits the tonic spiking, the blue color (region III) denotes the initial bursting, the black color (region IV) exhibits the irregular bursting, and the yellow color (region V) corresponds to the parameters that generate the regular bursting. Figure 2(b) displays the w_r bifurcation diagram for
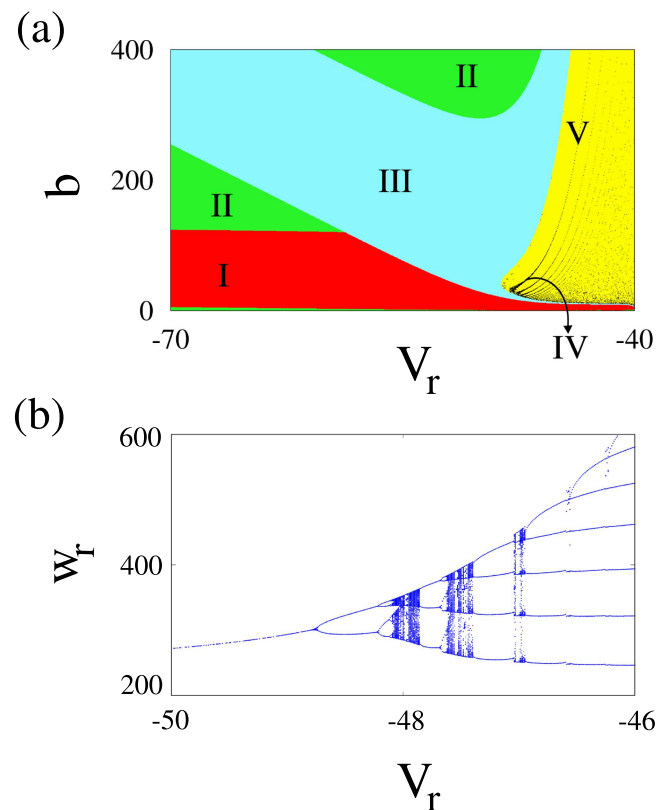
FIG. 2. Reset parameter space and bifurcation diagram of the Adex model. (a) Parameter space of the firing patterns where each region represents one firing pattern. Regions I, II, III, IV, and V exhibit adaptation spiking, tonic spiking, initial bursting, irregular bursting, and regular bursting firing patterns, respectively. (b) Bifurcation diagram of the Adex model. In panel (b), we plot w_r as a function of V_r for $b = 80$ pA.

12 August 2024 20:53:05

different values of V_r. As V_r increases, there is a period-doubling bifurcation, with some periodic and chaotic regions.

III. FRACTAL ADEX MODEL

In this section, we present the extension of the adaptive exponential integrate-and-fire model by means of the fractal operator. We study the behavior of the Adex model when the same fractal order is applied to V and w. Moreover, we consider two different fractal orders, α for the fractal order of the membrane potential and β for the fractal order of the adaptation current.

A. Fractal Adex model with equal order

In this work, we consider the following definition of the fractal operator:

$$\frac{df}{dt^\alpha} = \lim_{t_1 \to t} \frac{f(t_1) - f(t)}{(t_1 - t_0)^\alpha - (t - t_0)^\alpha} = \frac{1}{\alpha(t - t_0)^{\alpha-1}} \frac{df}{dt}, \quad (7)$$

as $t_0 = 0$,

$$\frac{df}{dt^\alpha} = \frac{1}{\alpha} t^{1-\alpha} \frac{df}{dt}, \quad (8)$$

where $\alpha > 0$ is the fractal order. This definition is known as Hausdorff derivative.[46] Considering the model described by Eqs. (1) and (2), our proposed extension becomes

$$C \frac{dV}{dt^\alpha} = -g_L(V - E_R) + g_L \Delta_T \exp\left(\frac{V - V_T}{\Delta_T}\right) - w + I, \quad (9)$$

$$\tau_w \frac{dw}{dt^\alpha} = a(V - E_R) - w. \quad (10)$$

Using the fractal derivative definition Eq. (8), we rewrite the fractal Adex model as

$$C \frac{dV}{dt} = \alpha t^{\alpha-1} \left[-g_L(V - E_R) + g_L \Delta_T \exp\left(\frac{V - V_T}{\Delta_T}\right) - w + I \right], \quad (11)$$

$$\tau_w \frac{dw}{dt} = \alpha t^{\alpha-1} \left[a(V - E_R) - w \right], \quad (12)$$

where the constants are rewritten in order to preserve the system units.

We observe that the reduction of the fractal order can increase the effect of the adaptation for spiking patterns. Figures 3(a)–3(c) show the potential membrane (V) as a function of the time (t) for $V_r = -68$ mV and $b = 60$ pA. Decreasing the value of α, the value of ISI between the firings increases. Reducing α to even smaller values, the neuron ceases its activity. For $\alpha > 1.0$, the intervals are shorter. However, the neuron hyperpolarises to unrealistic values.[58] To obtain biological solutions, we consider $0.7 \leq \alpha \leq 1.0$.

For the burst firing pattern, Figs. 3(g)–3(i), the reduction of the fractal order increases the inter-burst intervals. The fractal Adex model for a regular bursting pattern is shown in Figs. 3(g)–3(i). Panels (g) is computed for $\alpha = 1$, (h) is computed for $\alpha = 0.8$, and (i) is computed for $\alpha = 0.7$. The firing pattern does not change by reducing α, although the interval between each burst train changes. The intervals between each burst train increase considerably.
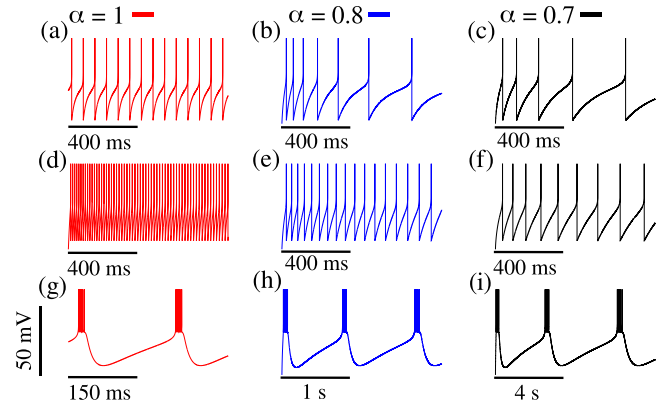
FIG. 3. Time evolution of the membrane potential of adaptive [(a)–(c)], tonic [(d)–(f)], and regular burst [(g)–(i)] patterns for three different values of α. We consider $\alpha = 1$ in panels (a), (d), and (g); $\alpha = 0.8$ in panels (b), (e), and (h); and $\alpha = 0.7$ in panels (c), (f), and (i). The reset parameters we considered are in Table I.

Most of the firing patterns do not change with α reduction; however, the tonic spiking does change. To show that, we consider the tonic spike firing pattern and reduce the fractal order. Figures 3(d)–3(f) depict the temporal evolution of the membrane potential. In panel (d), $\alpha = 1$ is associated with the tonic spike of the standard Adex model. The inter-spike intervals are quite similar over time. In panels (d)–(f), the reduction of fractal order to $\alpha = 0.7$ generates an adaptation of the spikes over time. Reducing even more the fractal order generates an increase in the adaptability of the firing patterns, which in this case is characterized by the adaptive spiking. In this way, the tonic firing pattern goes to adaptive spiking, where the fractal order less than the unity acts as an adaptation mechanism in the neuron, increasing the influence of adaptation current in the model.

Figure 4 exhibits the reset space parameter for $\alpha = 0.7$. The reset parameter space of the standard Adex model [Fig. 2(a)] and reset parameter space of $\alpha = 0.7$ (Fig. 4) are very similar in terms of the firing patterns. However, there are no tonic spiking regions in Fig. 4. The tonic spiking becomes adaptive as α reduces. For $0.7 \leq \alpha < 1$, the reset parameter space does not change in Fig. 4. For $\alpha = 1$, the reset parameter space is the same as the standard Adex model, displayed in Fig. 2. The sudden change from Figs. 2–4 is due to the effect of α on the interspike interval, which has a major effect on the tonic spiking region.

Although the firing pattern does not change for all patterns, the inter-spike intervals change and depend on the value of α, as shown in Fig. 3. Figure 5 displays $\overline{\text{ISI}}$ in log scale as a function of α for the firing patterns, distinguished by the color and point type. The blue squares are for $V_r = -68$ mV and $b = 60$ pA, the black circles are for $V_r = -47.4$ mV and $b = 41$ pA, the red triangles are for $V_r = -45$ mV and $b = 40$ pA, and the green stars are for $V_r = -65$ mV and $b = 5$ pA.

Independent of the reset parameters, $\overline{\text{ISI}}$ changes in a similar way. Figure 5 shows that such variation follows an exponential function, $\propto \exp(s\alpha)$, where s is the slope and is displayed in Table II.
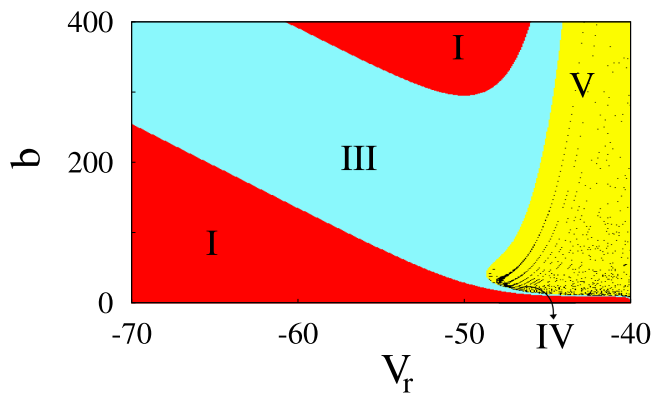
FIG. 4. Reset parameter space for $\alpha = 0.7$. Region I corresponds to the adaptive spiking, region III is related to the initial bursting, region IV is associated with the irregular bursting, and region V corresponds to the regular bursting.

The correlation coefficient indicates that the exponential function describes how $\overline{\text{ISI}}$ changes as α decreases. The four slopes of lines are very similar, indicating that $\overline{\text{ISI}}$ variation does not strongly depend on the reset parameters considered.

B. Fractal Adex model with two fractal orders

Now, we study the model dynamics when the fractal order is considered independently in V and w, as well as α and β. Both fractal orders are in the same range, $0.7 \leq \alpha \leq 1$ and $0.7 \leq \beta \leq 1$. The model is given by Eqs. (13) and (14),

$$C\frac{dV}{dt} = \alpha t^{\alpha-1}\left[-g_L(V - V_R) + g_L\Delta_T \exp\left(\frac{V - V_T}{\Delta_T}\right) - w + I\right],$$
(13)
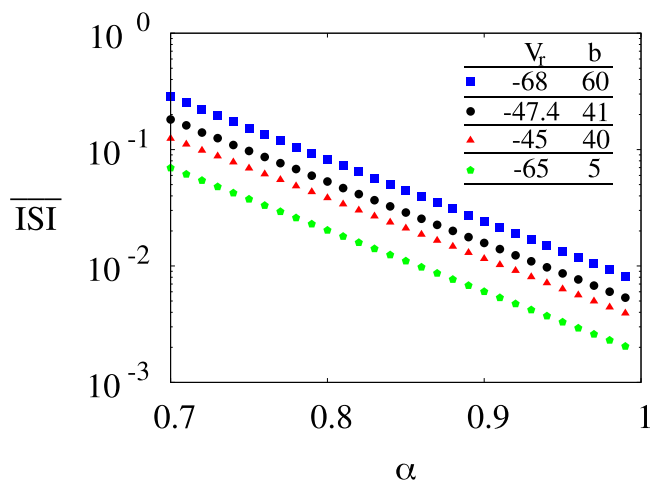
FIG. 5. $\overline{\text{ISI}}$ vs α for different firing patterns. The $\overline{\text{ISI}}$ values decrease exponentially with the reduction of α. The reset values are shown in Table I and the slopes in Table II.

TABLE II. Slopes of the reset parameters considered in Fig. 5.

Reset parameter (V_r, b)	s	Correlation coefficient
$(-68, 60)$	-12.23	0.999 97
$(-47.4, 41)$	-12.16	0.999 98
$(-45, 40)$	-11.95	0.999 98
$(-65, 5)$	-12.14	0.999 98

$$\tau_w\frac{dw}{dt} = \beta t^{\beta-1}\left[a(V - V_R) - w\right].$$
(14)

Figures 6(a)–6(c) display A, CV, and $\overline{F}$, respectively, for tonic spiking reset conditions, considering the parameters shown in Table I. In panel (a), we observe that A increases as α and β reduce. A increases at a faster rate with the reduction of β. The adaptive index reaches greater values than the critical value ($A_c = 0.01$), then characterizing the adaptive spiking firing pattern. To increase spiking adaptability, it is necessary to reduce at least one fractal order. Based on these results, we verify that the fractal order has a large influence on the neuron adapting mechanism. In panel (b), we observe that CV increases with the reduction of the (α, β), it happens due to the impact of fractal order in the $\overline{\text{ISI}}$. However, its increase does not surpass the CV threshold which characterizes bursting (CV ≥ 0.5). Panel (c) shows the mean firing rate parameter space. The reduction of the mean firing rate was expected due to the increase in the $\overline{\text{ISI}}$ occasioned by the fractal order.

The firing pattern depends on the fractal orders (α, β) considered as shown in Figs. 7(a) and 7(b). In panel (a), it is considered $V_r = -45$ mV and $b = 40$ pA (which characterize regular bursting in the standard model). A transition from regular bursting (region V) to initial bursting (region III) is observable. Regular bursting activity is delimited by the brown line given by

$$f(\alpha) = 1.03\alpha + 0.088.$$
(15)

It is worth mentioning that Eq. (15) delimits the transition between regular to initial bursting in Fig. 7(a). This result shows that distinct fractal order, α and β, changes the firing patterns. Therefore, in the extended model, the firing patterns depend not only on the reset parameter but also on fractal orders. For adaptation reset parameters in Fig. 2(a), the space parameter of $\beta \times \alpha$ does not change from the adaptive spike. However, the $\overline{\text{ISI}}$ increases. Considering tonic spiking reset parameters in Fig. 2(a), the $\beta \times \alpha$ parameter space shows the transition of tonic to adaptive spiking. Meanwhile, regular bursting reset parameters of Fig. 2(a) produce a transition between firing patterns in the $\alpha \times \beta$ parameter space.

Considering $V_r = -47.4$ mV and $b = 41$ pA (which characterize irregular bursting in the standard Adex model), the results show four distinct patterns for different pairs of (α, β), as shown in Fig. 7(b). Region I (red color) displays the adaptive spiking, region III (blue color) corresponds to the initial bursting, region IV (black color) is related to the irregular bursting, and region V (yellow color) shows the regular bursting. Different combinations of (α, β) transform the irregular firing pattern into regular bursting. The firing pattern stays as irregular bursting for pairs of α and β within the band defined by the functions $s(\alpha)$ and $k(\alpha)$, green and
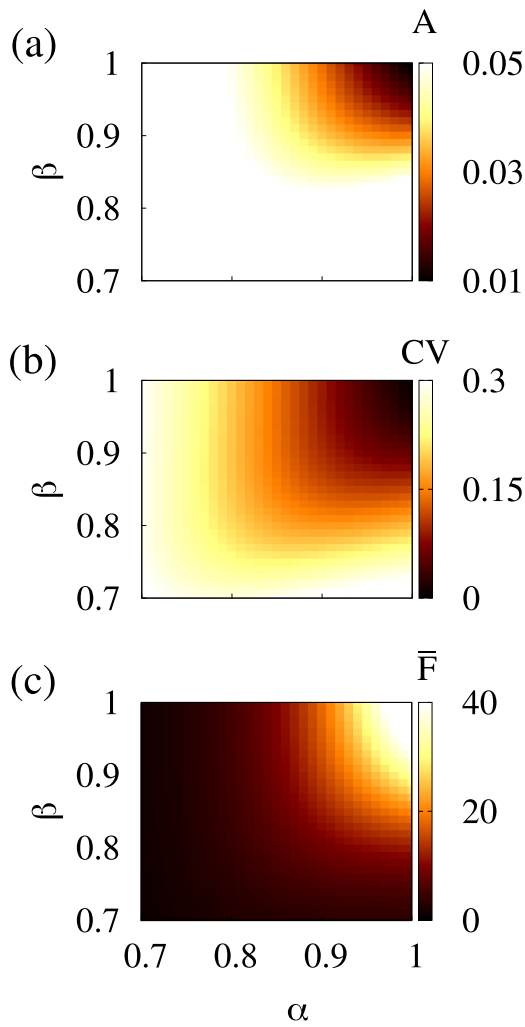
FIG. 6. Parameter space $\beta \times \alpha$. The color bars correspond to (a) adaptive index, (b) CV, and (c) mean firing rate. We consider $V_r = -65$ and $b = 5$, tonic spiking for the standard Adex model.
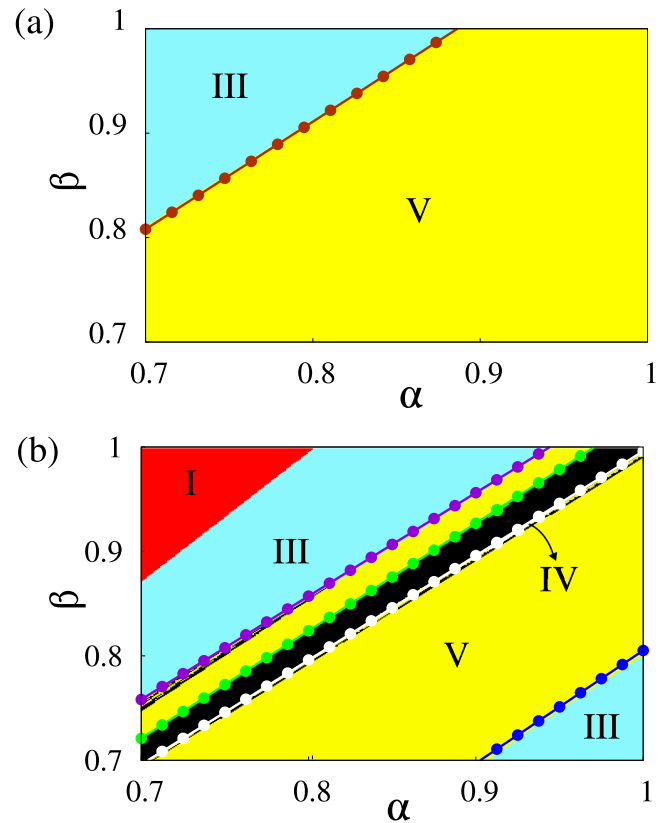

FIG. 7. Parameter space $\beta \times \alpha$ for (a) $V_r = -45$ mV and $b = 40$ pA and (b) $V_r = -47.4$ mV and $b = 41$ pA according to Table I. Region I shows the adaptive spiking pattern, region III corresponds to the initial bursting, region IV exhibits the irregular bursting, and region V shows the regular bursting. The dotted lines are the boundaries of bursting. The brown dotted line in (a) is the regular bursting boundary. The dotted line in panel (b) is the boundary of the irregular and regular bursting firing patterns. The purple and blue lines are the boundaries of regular bursting, superior [$g(\alpha)$], and inferior [$q(\alpha)$], respectively. The green and white dotted lines are irregular bursting boundaries, superior [$s(\alpha)$], and inferior [$k(\alpha)$], respectively.

white line, respectively,

$$k(\alpha) = \alpha - 0.004, \tag{16}$$

$$s(\alpha) = 1.03\alpha. \tag{17}$$

For $k(\alpha) \leq \beta \leq s(\alpha)$, the firing pattern is the same in the case $\alpha = \beta = 1$. There are transitions between regular and initial bursting. Initial bursting is easily achieved with α reduction. Considering $\beta = 1$, initial bursting is achieved for $\alpha = 0.94$. Meanwhile, if we consider $\alpha = 1$ initial bursting is firstly observed at $\beta = 0.8$. Fractal order α has more influence in the ceasing of bursting, it is possible to generate initial bursting with a higher value of α. The bursting inferior boundary is given by (blue dotted line)

$$q(\alpha) = 1.08\alpha - 0.275, \tag{18}$$

and the superior (purple dotted line) by

$$g(\alpha) = \alpha + 0.059. \tag{19}$$

Another transition occurs from regions III to I, where the boundary is defined by

$$r(\alpha) = 1.24\alpha + 0.003. \tag{20}$$

The reset parameters influence how α and β change the firing patterns, Fig. 8. The panel (a) shows $\alpha \times \beta$ parameter space for three different values of V_r. Small increments of this reset parameter add more firing pattern regions. For $V_r = -57.5$ only adaptive spiking is seen (red region). For $V_r = -52.5$, two regions are seen, the red region (adaptive) and the blue region (initial bursting). Considering $V_r = -47.5$, four firing patterns appear, red region (adaptive spiking), blue region (initial bursting), yellow region (regular bursting), and black region (irregular bursting). The variation of the
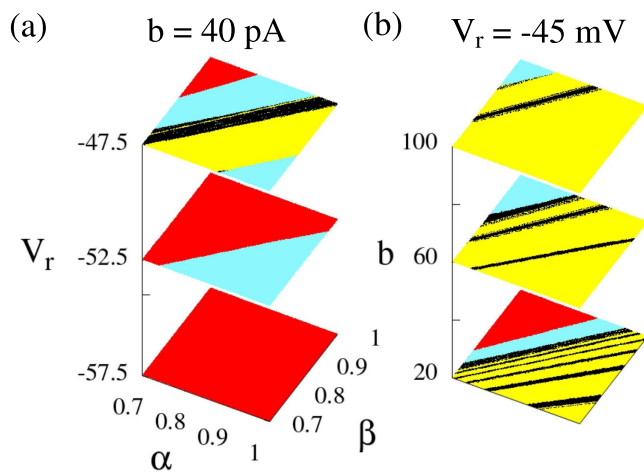
FIG. 8. $\alpha \times \beta$ parameter space for different combinations of reset parameters. (a) We fix the reset parameter $b = 40$ pA and vary V_r, and (b) we fix $V_r = -45$ mV and vary b.

reset potential influences the initial, regular, and irregular bursting appearance in (α, β) space parameter. The panel (b) shows (α, β) parameter spaces for three values of b for $V_r = -45$ mV. b increment has the opposite effect of V_r increase, higher values of b reduce the amount of firing patterns seen in the parameter space. For $b = 20$ pA, four different firing pattern regions are shown, red region is the adaptive spiking, blue region initial bursting, yellow region regular bursting, and black region irregular bursting. For $b = 60$ and $b = 100$ pA, only three firing patterns are generated. However, the irregular bursting pattern regions reduce for $b > 20$ pA.

These results, combined with the ones presented in Fig. 6, reinforce that different firing patterns are not only produced by V_r and b but also by the non-integer order of the extended operator. Both orders influence the model dynamics, the fractal order β greatly affects the adaptability of the neuron. However, the potential membrane fractal order α has greater influences on the firing pattern transition of bursting to spiking.

IV. DISCUSSION AND CONCLUSION

In this work, we proposed and studied the adaptive exponential integrate-and-fire (Adex) model with fractal extension. We noticed that the fractal order Adex is capable of reproducing neuronal activity as the Adex standard model. However, differently from the standard one, the fractal order presents quantitative differences in the adaptability, firing frequency, and variability of the inter-spike intervals. When the same fractal order is considered in both variable evolution related to the membrane potential (V) and adaptation current (w), the reduction of the fractal order in the membrane potential derivative reduces the tonic spike firing pattern in the studied parameters space. The reduction of the fractal order works to make the spike firing difficult, i.e., when α is reduced the firing frequency becomes lower. Moreover, our results also suggest

that the mean inter-spike intervals follow an exponential law as a α function.

In addition, when the fractal order is considered independently in V and w, we observed that the reduction of the fractal order in the adaptation current generated a larger effect than in the potential variable, increasing the adaptability in the firing patterns. In our simulations, the reduction in the fractal order in an independent way produces similar magnitude changes in the coefficient of variation and mean firing frequency. In particular, we highlight the transition from tonic spike to adaptive spiking due to the reduction of the fractal order. We also concluded that, depending on the combination of fractal order in the variables, the model can exhibit other patterns, however, as the main result, the tonic spike is reduced or absent as a consequence of order reduction.

Equations (15) and (17) are very similar, their only difference is the independent term 0.088 in Eq. (15). Their slope is the same, which shows that the transition of the patterns in both cases occurs at the same rate of variation of the fractal orders. Considering $\alpha = 0.7$, the transition of initial to regular bursting in Fig. 7(a) occurs at $\beta = 0.809$. The independent term in Eq. (15) plays a crucial role in the value in which this transition happens. The other boundaries are not as similar as Eqs. (15) and (17), their slopes and independent terms vary. These boundary equations limit the values of (α, β) in which regular and irregular bursting are observable. Therefore, it is possible to select a combination of (α, β) to describe the desired firing pattern. In future works, we plan to study a way of generalization of the bursting boundaries for any reset parameters to expand the applicability of these equations.

When fractal derivatives are considered, their orders influence the firing pattern similarly to the reset parameters in the standard model. Two sets of parameters are necessary to achieve different firing patterns, the reset parameters (V_r, b) and the fractal orders (α, β). (V_r, b) change the firing pattern parameter space of $\alpha \times \beta$ and vice versa. However, the parameters act differently in each parameter space. (α, β) increase the mean interspike interval and suppress the emergence of tonic spiking, and the reset parameter b reduces the amount of firing pattern shown in $\alpha \times \beta$ parameter space.

The AdEx model has the advantage of using few parameters to reproduce experimental data. In particular, it is possible to obtain six different types of firing patterns by varying just two parameters (V_r and b). The parameter b is related to adaptation and can be varied to better represent the temporal evolution of ISIs of a neuron. On the other hand, the parameter V_r estimates the value of the membrane potential after an action potential. This parameter can be measured directly from voltage traces and cannot be arbitrarily changed. It is observed that cells with the same value of V_r can exhibit different adaptation levels, firing patterns, and frequencies.[16] For this reason, it is necessary to include new parameters to accommodate this firing diversity. We show how the Adex model with fractal extension enables a better representation of the adaptability, variability, and frequency of firing patterns, in this way expanding the applicability of the Adex model. In future works, we plan to use the fractal orders as a means of fitting experimental data of single neurons to neuronal networks, expanding the model and its applicability for more general situations and also to better understand some brain disorders.

With respect to the order of fractal derivatives, our study also encountered some limitations. The meaningful solutions in terms of biological plausibility are found in the range $\alpha \in (0.7, 1]$. Although our results are revealing regarding the potential effect of fractal order in single neurons, more investigation into the effect of fractal order on the dynamics of neuronal networks is necessary. In conclusion, our study provides clear evidence of the influence of the fractal order in the firing patterns and frequency of the Adex neuron model. Our results expand the applicability of the Adex model, supporting future investigations considering the fractal order neuron models.

AUTHOR DECLARATIONS

Conflict of Interest

The authors have no conflicts to disclose.

Author Contributions

Diogo L. M. Souza: Conceptualization (equal); Data curation (equal); Formal analysis (equal); Investigation (equal); Methodology (equal); Software (equal); Validation (equal); Visualization (equal); Writing – original draft (equal); Writing – review & editing (equal). **Enrique C. Gabrick:** Conceptualization (equal); Formal analysis (equal); Investigation (equal); Methodology (equal); Software (equal); Validation (equal); Visualization (equal); Writing – original draft (equal); Writing – review & editing (equal). **Paulo R. Protachevicz:** Conceptualization (equal); Formal analysis (equal); Investigation (equal); Methodology (equal); Software (equal); Validation (equal); Visualization (equal); Writing – original draft (equal); Writing – review & editing (equal). **Fernando S. Borges:** Conceptualization (equal); Formal analysis (equal); Investigation (equal); Methodology (equal); Software (equal); Validation (equal); Visualization (equal); Writing – original draft (equal); Writing – review & editing (equal). **José Trobia:** Conceptualization (equal); Formal analysis (equal); Investigation (equal); Methodology (equal); Software (equal); Validation (equal); Visualization (equal); Writing – original draft (equal); Writing – review & editing (equal). **Kelly C. Iarosz:** Conceptualization (equal); Formal analysis (equal); Investigation (equal); Methodology (equal); Software (equal); Validation (equal); Visualization (equal); Writing – original draft (equal); Writing – review & editing (equal). **Antonio M. Batista:** Conceptualization (equal); Formal analysis (equal); Methodology (equal); Software (equal); Supervision (equal); Validation (equal); Visualization (equal); Writing – original draft (equal); Writing – review & editing (equal). **Iberê L. Caldas:** Conceptualization (equal); Formal analysis (equal); Funding acquisition (equal); Methodology (equal); Software (equal); Supervision (equal); Validation (equal); Visualization (equal); Writing – original draft (equal); Writing – review & editing (equal). **Ervin K. Lenzi:** Conceptualization (equal); Formal analysis (equal); Investigation (equal); Methodology (equal); Software (equal); Supervision (equal); Validation (equal); Visualization (equal); Writing – original draft (equal); Writing – review & editing (equal).

DATA AVAILABILITY

The data that support the findings of this study are available within the article.

REFERENCES

[1] R. B. Northrop, *Introduction to Dynamic Modeling of Neuro-Sensory Systems* (CRC Press, 2001).

[2] W. Gerstner, W. M. Kistler, R. Naud, and L. Paninski, *Neuronal Dynamics: From Single Neurons to Networks and Models of Cognition*, 1st ed. (Cambridge University Press, Cambridge, 2014).

[3] A. L. Hodgkin and A. F. Huxley, "A quantitative description of membrane current and its application to conduction and excitation in nerve," J. Physiol. **117**, 500 (1952).

[4] J. L. Hindmarsh and R. M. Rose, "A model of neuronal bursting using three coupled first order differential equations," Proc. R. Soc. London, Ser. B **221**, 87 (1984).

[5] E. M. Izhikevich, "Resonate-and-fire neurons," Neural Networks **14**, 883–894 (2001).

[6] L. Abbott, "Lapicque's introduction of the integrate-and-fire model neuron (1907)," Brain Res. Bull. **50**, 303–304 (1999).

[7] R. Brette and W. Gerstner, "Adaptive exponential integrate-and-fire model as an effective description of neuronal activity," J. Neurophysiol. **94**, 3637–3642 (2005).

[8] N. F. Rulkov, "Regularization of synchronized chaotic bursts," Phys. Rev. Lett. **86**, 183–186 (2001).

[9] F. S. Borges, J. V. S. Moreira, L. M. Takarabe, W. W. Lytton, and S. Dura-Bernal, "Regularization of synchronized chaotic bursts," Front. Neuroinf. **16**, 884245 (2022).

[10] R. L. Viana, F. Borges, K. C. Iarosz, A. M. Batista, S. R. Lopes, and I. L. Caldas, "Dynamic range in a neuron network with electrical and chemical synapses," Commun. Nonlinear Sci. Numer. Simul. **19**, 164–172 (2014).

[11] F. S. Borges, E. L. Lameu, A. M. Batista, K. C. Iarosz, M. S. Baptista, and R. L. Viana, "Complementary action of chemical and electrical synapses to perception," Physica A **430**, 236–241 (2015).

[12] O. Kinouchi and M. M. Copelli, "Optimal dynamical range of excitable networks at criticality," Nat. Phys. **2**, 348–351 (2006).

[13] E. Sayari, A. M. Batista, E. C. Gabrick, K. C. Iarosz, M. Hansen, J. D. Szezech, Jr., and F. S. Borges, "Dynamics of a perturbed random neuronal network with burst-timing-dependent plasticity," Eur. Phys. J. Spec. Top. **231**, 4049–4056 (2022).

[14] E. Sayari, E. C. Gabrick, F. S. Borges, F. E. Cruzaniani, P. R. Protachevicz, K. C. Iarosz, J. D. Szezech, Jr., and A. M. Batista, "Analyzing bursting synchronization in structural connectivity matrix of a human brain under external pulsed currents," Chaos **33**, 033131 (2023).

[15] F. S. Borges, E. C. Gabrick, P. R. Protachevicz, G. S. V. Higa, E. L. Lameu, P. X. R. Rodriguez, M. S. A. Ferraz, J. D. Szezech, Jr., A. M. Batista, and A. H. Kihara, "Intermittency properties in a temporal lobe epilepsy model," Epilepsy Behav. **139**, 109072 (2023).

[16] R. Naud, N. Marcille, C. Clopath, and W. Gerstner, "Firing patterns in the adaptive exponential integrate-and-fire model," Biol. Cybern. **99**, 335–347 (2008).

[17] F. S. Borges, P. R. Protachevicz, E. L. Lameu, R. C. Bonetti, K. C. Iarosz, I. L. Caldas, M. S. Baptista, and A. M. Batista, "Synchronised firing patterns in a random network of adaptive exponential integrate-and-fire neuron model," Neural Networks **90**, 1–7 (2017).

[18]L. Hertag, J. Hass, T. Golovko, and D. Durstewitz, "An approximation to the adaptive exponential integrate-and-fire neuron model allows fast and predictive fitting to physiological data," Front. Comput. Neurosci. **6**, 62 (2012).

[19]R. Brette, "What is the most realistic single- compartment model of spike initiation?," PLoS Comput. Biol. **11**, e1004114 (2015).

[20]J. Touboul and R. Brette, "Dynamics and bifurcations of the adaptive exponential integrate-and-fire model," Biol. Cybern. **99**, 319–334 (2008).

[21]P. R. Protachevicz, F. S. Borges, E. L. Lameu, P. Ji, K. C. Iarosz, A. H. Kihara, I. L. Caldas, J. D. Szezech, Jr., M. S. Baptista, E. N. Macau, C. G. Antonopoulos, A. M. Batista, and J. Kurths, "Bistable firing pattern in a neural network model," Front. Comput. Neurosci. **13**, 19 (2019).

[22]J. D. Templos-Hernández, L. A. Quezada-Téllez, B. M. González-Hernández, G. Rojas-Vite, J. E. Pineda-Sánchez, G. Fernández-Anaya, and E. E. Rodriguez-Torres, "A fractional-order approach to cardiac rhythm analysis," Chaos, Solitons Fractals **147**, 110942 (2021).

[23]H. Jafari, R. M. Ganji, N. S. Nkomo, and Y. P. Lv, "A numerical study of fractional order population dynamics model," Res. Phys. **27**, 104456 (2021).

[24]E. C. Gabrick, E. Sayari, A. S. M. de Castro, J. Trobia, A. M. Batista, and E. K. Lenzi, "Fractional Schrödinger equation and time dependent potentials," Commun. Nonlinear Sci. Numer. Simul. **123**, 107275 (2023).

[25]E. K. Lenzia, E. C. Gabrick, E. Sayari, A. S. M. de Castro, J. Trobia, and A. M. Batista, "Anomalous relaxation and three-level system: A fractional Schrödinger equation approach," Quantum Rep. **5**, 442–458 (2023).

[26]V. E. Tarasov, "Fractional generalization of gradient and Hamiltonian systems," J. Phys. A: Math. Gen. **38**, 5929 (2005).

[27]A. Somer, A. Novatski, M. K. Lenzi, L. R. da Silva, and E. K. Lenzi, "Photothermal response for the thermoelastic bending effect considering dissipating effects by means of fractional dual-phase-lag theory," Fractal Fract. **7**, 276 (2023).

[28]C. M. A. Pinto, A. R. M. Carvalho, and J. N. Tavares, "Time-varying pharmacodynamics in a simple non-integer HIV infection model," Math. Biosci. **307**, 1–12 (2019).

[29]V. E. Tarasov, "Mathematical economics: Application of fractional calculus," Mathematics **8**, 660 (2020).

[30]S. Arora, T. Mathur, S. Agarwal, K. Tiwari, and P. Gupta, "Applications of fractional calculus in computer vision: A survey," Neurocomputing **489**, 407–428 (2022).

[31]A. Giusti, "General fractional calculus and Prabhakar's theory," Commun. Nonlinear Sci. Numer. Simul. **83**, 105114 (2020).

[32]F. Brouers and T. J. Al-Musawi, "Brouers-Sotolongo fractal kinetics versus fractional derivative kinetics: A new strategy to analyze the pollutants sorption kinetics in porous materials," J. Hazard. Mater. **350**, 162–168 (2018).

[33]W. Chen, H. Sun, X. Zhang, and D. Korosak, "Anomalous diffusion modeling by fractal and fractional derivatives," Comput. Math. Appl. **59**, 1754–1758 (2010).

[34]Q. Wang, J. He, and Z. Li, "Fractional model for heat conduction in polar bear hairs," Therm. Sci. **16**, 339–342 (2012).

[35]J. A. He, "A tutorial review on fractal spacetime and fractional calculus," Int. J. Theor. Phys. **326**, 3698–3718 (2014).

[36]D. Jun, Z. Guang-jun, X. Yong, Y. Hong, and W. Jue, "Dynamic behavior analysis of fractional-order Hindmarsh–Rose neuronal model," Cognit. Neurodyn. **8**, 167–175 (2014).

[37]Y. Yu, M. Shi, M. C. H. Kang, and B. Bao, "Hidden dynamics in a fractional-order memristive Hindmarsh–Rose model," Nonlinear Dyn. **100**, 891–906 (2020).

[38]A. M. Nagy and N. H. Sweilam, "An efficient method for solving fractional Hodgkin–Huxley model," Phys. Lett. A **378**, 1980–1984 (2014).

[39]S. H. Weinberg, "Membrane capacitive memory alters spiking in neurons described by the fractional-order Hodgkin-Huxley model," PLoS One **10**, e0126629 (2015).

[40]Y. M. Lu, C. H. Wang, Q. L. Deng, and C. Xu, "The dynamics of a memristor-based rulkov neuron with fractional-order difference," Chin. Phys. B **31**, 060502 (2022).

[41]M. Ma, Y. Lu, Z. Li, Y. Sun, and C. Wang, "Multistability and phase synchronization of rulkov neurons coupled with a locally active discrete memristor," Fractal Fract. **7**, 82 (2023).

[42]W. W. Teka, R. K. Upadhayay, and A. Mondal, "Fractional-order leaky integrate-and-fire model with long-term memory and power law dynamics," Neural Networks **93**, 110–125 (2017).

[43]W. Teka, T. M. Marinov, and F. Santamaria, "Neuronal spike timing adaptation described with a fractional leaky integrate-and-fire model," PLoS Comput. Biol. **10**, e100326 (2014).

[44]W. Chen, "Time–space fabric underlying anomalous diffusion," Chaos, Solitons Fractals **28**, 923–929 (2006).

[45]W. Chen, F. Wang, B. Zheng, and W. Cai, "Non-Euclidean distance fundamental solution of Hausdorff derivative partial differential equations," Eng. Anal. Boundary Elem. **84**, 213–219 (2017).

[46]J. H. He, "Fractal calculus and its geometrical explanation," Res. Phys. **10**, 272–276 (2013).

[47]W. Chen, Y. Liang, and W. Cai, *Hausdorff Calculus: Applications to Fractal Systems* (De Gruyter, 2019), pp. 1–148.

[48]L. Nottale, "On time in microphysics," Acad. Sci. Paris C. R. Ser. Sci. Math. **306**, 341–346 (1988).

[49]A. B. Hamissa, F. Brouers, A. M. C. Ncibi, and M. Seffen, "Kinetic modeling study on methylene blue sorption onto science Agave americana fibers: Fractal kinetics and regeneration studies," Sep. Sci. Technol. **48**, 2834–2842 (2013).

[50]A. M. B. Hamissa, F. Brouers, B. Mahjoub, and M. Seffen, "Adsorption of textile dyes using agave americana (l.) fibres: Equilibrium and kinetics modelling," Adsort. Sci. Technol. **25**, 311–325 (2007).

[51]S. Figaro, J. P. Avril, F. Brouers, A. Ouensanga, and S. Gaspard, "Adsorption studies of molasse's wastewaters on activated carbon: Modelling with a new fractal kinetic equation and evaluation of kinetic models," J. Hazard. Mater. **161**, 649–656 (2009).

[52]M. S. E. Naschie, L. Marek-Crnjac, J. H. He, and M. A. Helal, "Computing the missing dark energy of a clopen universe which is its own multiverse in addition to being both flat and curved," Fractal Spacetime Noncommut. Geom. Quantum High Energy Phys. **3**, 3–10 (2013).

[53]M. S. E. Naschie, "A unified newtonian-relativistic quantum resolution of the supposedly missing dark energy of the cosmos and the constancy of the speed of light," Int. J. Mod. Nonlinear Theory Appl. **2**, 43–54 (2013).

[54]E. C. Gabrick, E. Sayari, D. L. Souza, F. S. Borges, J. Trobia, E. K. Lenzi, and A. M. Batista, "Fractal and fractional SIS model for syphilis data," Chaos **33**, 093124 (2023).

[55]A. Atangana and S. Qureshi, "Modeling attractors of chaotic dynamical systems with fractal–fractional operators," Chaos, Solitons Fractals **123**, 320–337 (2019).

[56]F. Gabbiani and C. C. Koch, "Principles of spike train analysis," in *Methods in Neuronal Modeling: From Ions to Networks*, 2nd ed., edited by C. Koch and I. Segev (MIT Press, Cambridge, 1998), pp. 313–360.

[57]T. Fardet, M. Ballandras, S. Bottani, S. Métens, and P. Monceaus, "Understanding the generation of bursts by adaptive oscillatory neurons," Front. Neurosci. **12**, 41 (2018).

[58]D. Brown and P. Adams, "Muscarinic suppression of a novel voltage-sensitive k^+ current in a vertebrate neurone," Nature **283**, 673–676 (1980).